Properties and Crystal Structure of a β-Barrel Folding Mutant

Ira J. Ropson,* Brian C. Yowler,* Paula M. Dalessio,* Leonard Banaszak,† and James Thompson†
*Department of Biochemistry and Molecular Biology, Penn State University College of Medicine, Hershey, Pennsylvania 17033; and
†Department of Biochemistry, Molecular Biology, and Biophysics, University of Minnesota, Minneapolis, Minnesota 55455 USA

ABSTRACT A mutant of a β-barrel protein, rat intestinal fatty acid binding protein, was predicted to be more stable than the wild-type protein due to a novel hydrogen bond. Equilibrium denaturation studies indicated the opposite: the V60N mutant protein was less stable. The folding transitions followed by CD and fluorescence were reversible and two-state for both mutant and wild-type protein. However, the rates of denaturation and renaturation of V60N were faster. During unfolding, the initial rate was associated with 75–80% of the fluorescence and all of the CD amplitude change. A subsequent rate accounted for the remaining fluorescence change for both proteins; thus the intermediate state lacked secondary structure. During folding, one rate was detected by both fluorescence and CD after an initial burst phase for both wild-type and mutant. An additional slower folding rate was detected by fluorescence for the mutant protein. The structure of the V60N mutant has been obtained and is nearly identical to prior crystal structures of IFABP. Analysis of mean differences in hydrogen bond and van der Waals interactions did not readily account for the stability loss due to the mutation. However, significant average differences of the solvent accessible surface and crystallographic displacement factors suggest entropic destabilization.

INTRODUCTION

Rat intestinal fatty acid binding protein (IFABP) is a small β-barrel protein that binds a single fatty acid within a relatively large interior cavity near the center of the barrel (Fig. 1). The tertiary structure is common to the intracellular lipid binding protein family and is representative of a large set of homologous structures (Banaszak et al., 1994). The family members are expressed in different tissues, and hence in addition to IFABP there is a heart form, liver form, and adipocyte form, all of which bind fatty acids (for reviews see Banaszak et al., 1994; Bass, 1993; Bernlohr et al., 1997). Other family members bind retinoids or other hydrophobic ligands, and the liver form is known to bind bile pigments and fatty acyl-CoA compounds as well as fatty acids (Banaszak et al., 1994; Bass, 1993).

There are only small conformational differences between the ligand-bound and apo-forms of these proteins. The cavity-binding site is larger than most ligands and has been shown to contain many partially immobilized waters, even when ligand is bound. Volume calculations indicate that this internal cavity may contain additional disordered water molecules as well. Therefore, much of the central interiors of these proteins are water-filled cavities rather than the usual hydrophobic core found in most proteins. About half the cavity surface, however, is formed by well-packed hydrophobic residues.

The folding of IFABP is simplified by the lack of any proline or cysteine residues. The equilibrium constants and rates for the reversible folding and unfolding of wild-type IFABP have been examined under a variety of conditions (Ropson et al., 1990; Ropson and Dalessio, 1997; Dalessio and Ropson, 1998; Dalessio and Ropson, 2000; Burns et al., 1998). At physiological pH the unfolding at equilibrium follows a simple two-state model, implying the absence of stable intermediate states. However, stopped-flow kinetic studies of unfolding in the presence of urea and guanidine hydrochloride were multiphasic, suggesting the presence of at least one intermediate. This state appeared to have little if any secondary structure associated with it (Ropson et al., 1990; Ropson and Dalessio, 1997; Dalessio and Ropson, 1998).

Double-jump experiments indicated that the intermediate is formed rapidly during refolding (Dalessio and Ropson, 2000). As such, a tertiary interaction involving one or both of the tryptophans in this protein are the last structures to break down during unfolding and the first structures formed during refolding. Current evidence suggests that this folding nucleus is at the bottom of the cavity, farthest from the two α-helices (Fig. 1). The region contains both local (four or fewer residues distant in the sequence) and nonlocal (more than four residues distant in the sequence) interactions.

An IFABP mutant in which a nonpolar side chain, V60, was replaced with an asparagine was made and found to affect both the stability and the folding mechanism of the protein. This site is adjacent to the internal ligand-binding pocket and thus conversion to a polar side chain could result in novel solvent interactions within the cavity. An asparagine is found at this location in two other proteins in this family, ileal lipid binding protein (Gantz et al., 1989), and liver fatty acid binding protein (Gordon et al., 1983). In liver fatty acid binding protein it projects toward the internal solvent cavity and forms two hydrogen bonds with nearby main-chain atoms. Modeling suggests an asparagine at this position in IFABP may orient to form both hydrogen bonds

Received for publication 9 September 1999 and in final form 22 December 1999.

Address reprint requests to Leonard Banaszak, Department of Biochemistry, Molecular Biology, and Biophysics, 4-225 Millard Hall, University of Minnesota, 435 Delaware St. S.E., Minneapolis, MN 55455. Tel.: 612-626-6597; Fax: 612-624-5121; E-mail: len_b@dcmir.med.umn.edu.

0006-3495/00/03/1551/10 $2.00

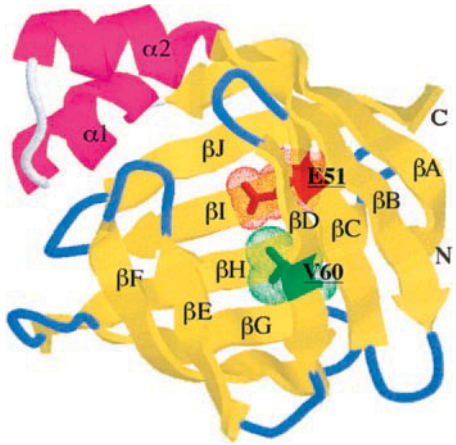

FIGURE 1 Cartoon structure of wild-type IFABP. The ribbon diagram describes the overall conformation of IFABP. Two helices capping the barrel-like structure are drawn in red and labeled αI and αII. Each of the 10 β-strands are labeled alphabetically beginning at the N-terminal. The location of the V60 and E51 are shown as sticks with a dot surface showing their van der Waals radii.

in a similar manner. In addition, a hydrogen bond with another polar residue located in the cavity, E51, appeared likely.

The V60N mutation is also in the gap region between the fourth and fifth strands of the β-barrel. These are marked by the symbols βD and βE in Fig. 1. The gap region does not contain the inter-strand hydrogen bonds normally found in a β-sheet structure. Water molecules and side chains bridge the space between these strands, keeping the barrel surface intact. If the ψ and ϕ angles at this site are changed by the mutation, the mutant asparagine side chain could interact with water molecules on the exterior of the protein or in this gap region, leaving the ~86 main-chain hydrogen bonds intact. As described below, this mutation had significant effects on the folding and stability of this protein, but the crystal structure of the mutant protein appeared very similar to other structures of wild-type IFABP.

METHODS

Protein source and purification

IFABP and V60N-IFABP were produced in *Escherichia coli*, purified to homogeneity, and delipidated as previously described (Lowe et al., 1987; Sacchettini et al., 1989; 1990; Ropson and Frieden, 1992). Dr. David Cistola (Washington University School of Medicine) generously provided a clone of V60N-IFABP. Protein purity was demonstrated by the presence of a single band on an SDS polyacrylamide gel. An extinction coefficient of 1.1 mg^{-1} cm^{-1} at 280 nm was used to determine IFABP concentration (Ropson et al., 1990).

Reagents

Denaturant stock solutions were prepared from ultrapure urea as previously described (Ropson and Dalessio, 1997). On the day of an experiment a 9 M urea solution containing 75 mM NaCl, 0.1 mM EDTA, and 25 mM sodium phosphate (pH 7) was made from a 10 M frozen stock. The final urea concentration was determined by refractive index measurements using a Milton Roy Abbe-3C refractometer at 25°C in conjunction with an equation relating refractive index to concentration (Pace, 1986). Buffers were filtered through a 0.22 μm membrane before use. Unless otherwise denoted, all chemicals were reagent grade.

Energy minimization

The structure and stability of the mutant protein was modeled using the crystal coordinates for apo IFABP (Protein Data Base (pdb) accession code: 1ifc). The mutation was made in silico using the Biopolymer module of the Insight II software suite (Molecular Simulations Inc., San Diego, CA). Energy minimization was performed using the Discover module of the Insight II software suite under default conditions with and without solvent using three different force fields (amber, cvff, cff91) for both the mutant and wild-type proteins. One picosecond molecular dynamics simulations were performed using the Discover module and the amber force field at 300 K for both the wild-type and mutant proteins without solvent, starting from the energy-minimized structure. Structures from both simulations were saved every 0.1 ps and minimized using the amber force field.

Equilibrium studies

Equilibrium unfolding transitions were monitored by circular dichroism (CD) and fluorescence spectroscopy as a function of denaturant concentration. A Jasco (Easton, MD) J-710 spectropolarimeter was used to follow the loss of secondary structure in the wavelength range of 225–212 nm using a thermostatted 0.1 mm cell. Fluorescence changes were followed with an Aminco-Bowman (Rochester, NY) Series 2 luminescence spectrometer with excitation at 290 nm (2 nm bandpass) and emission at 327 nm (8 nm bandpass) in a 1 cm thermostatted cell. All measurements were made at 25°C. Protein concentrations for CD and fluorescence experiments were usually 100 μg/ml. All experiments were repeated at least two times and agreed well. The parameter estimates were calculated using multiple data sets.

CD kinetic studies

The kinetics of unfolding and refolding were monitored by CD with a Jasco J-710 spectropolarimeter in conjunction with an RX1000 stopped-flow apparatus (Applied Photophysics, Ltd., London, UK) as previously described (Ropson and Dalessio, 1997). Kinetic time courses were followed at 218 nm. For all experiments, five parts of denaturant were mixed with one part of protein (0.52 mg/ml final concentration) and five to seven transients were averaged for each concentration of urea. Typical examples of individual time courses have been published for the wild-type protein (Ropson and Dalessio, 1997).

Fluorescence kinetic studies

The kinetics of unfolding and refolding was followed by fluorescence using an Applied Photophysics sequential DX-17MV stopped-flow spectrophotometer. Excitation was 290 nm (0.5 mm slits) using a 0.2 cm pathlength. The emission intensity was monitored above 305 nm at 90° through a WG305 Schott glass filter (Oriel, Stratford, CO) at 25°C. In both unfolding and refolding experiments, five parts of denaturant solution were mixed with one part protein solution (0.26 mg/ml, final concentration). The dead time for this instrument at this mixing ratio was determined to be 5–10 ms (Ropson and Dalessio, 1997). Data collected in the dead time range were discarded from the analysis. Typical examples of individual

time courses have been published for the wild-type protein (Ropson and Dalessio, 1997).

Fitting of equilibrium and kinetic data

Nonlinear least-squares interpretation of the equilibrium data were generated by using the KaleidaGraph (Synergy Software, Reading, PA) in conjunction with an equation adapted from Santoro and Bolen (1988):

$$X_{[D]} = \frac{\left\{(X_N + m_N[D]) + (X_U + m_U[D])\exp\left(-\frac{\Delta G_{H_2O}}{RT} + \frac{m_G[D]}{RT}\right)\right\}}{\left\{1 + \exp\left(-\frac{\Delta G_{H_2O}}{RT} + \frac{m_G[D]}{RT}\right)\right\}}$$

where $X_{[D]}$ is the value of the spectroscopic property at some denaturant concentration [D]; X_N and X_U are the values for the spectroscopic property linearly extrapolated to [D] = 0 for the native and unfolded forms of the protein, respectively; m_N and m_U are the slopes for the dependence of the spectroscopic properties X_N and X_U on denaturant concentration, respectively; ΔG_{H_2O} is the apparent free energy difference between the folded and unfolded forms of the protein linearly extrapolated to [D] = 0; m_G is the slope describing the dependence of ΔG_{H_2O} on [D], assuming a linear relationship between the log of the equilibrium constant and denaturant constant; R is the gas constant; and T is the temperature. The midpoint of the transition was determined by dividing ΔG_{H_2O} by m_G, or by substituting ΔG_{H_2O}/midpoint for m_G in the equation shown above.

The nonlinear least-squares regression program supplied by Applied Photophysics was used to determine the best fit of these kinetic data to the following rate equation:

$$A(t) = \sum_i A_i \exp(-k_i t) + A_\infty$$

where $A(t)$ is the amplitude of the change at time t, A_∞ is the amplitude at infinite time, A_i is the amplitude at zero time of phase i, and k_i is the rate of phase i formation. Stopped-flow CD data were fit to monophasic and biphasic decay equations using KaleidaGraph.

In all cases, the criteria of Mannervik (1982) and Motulsky and Ransnas (1987) were used to determine goodness-of-fit of the data to the various models. When the standard error of a parameter exceeded the value of that parameter determined by fitting, the parameter was eliminated from the equation, and the interpretation was repeated. This process of elimination was continued until all remaining terms were significant.

X-ray methods

Crystals were obtained by hanging-drop vapor diffusion at room temperature with a 6 μl droplet containing 4.6 mg/ml protein. The reservoirs contained 36–38% PEG 4000, 0.1 M PIPES at pH 7.3. The diffraction data were collected from two single crystals on a Siemens HiStar detector and processed with XENGEN software (Howard et al., 1987). The V60N mutant crystals were monoclinic belonging to the space group $P2_1$, and had cell dimensions of $a = 36.64$, $b = 52.37$, $c = 31.59$ Å, $\beta = 90.92°$. This crystal habit differs little from those previously reported for three of five IFABP entries in the pdb, each with a monomer in the asymmetric unit.

Despite the correspondence with three native crystal habits, molecular replacement was required to obtain starting phases due to non-isomorphic reflection intensities. The search model was derived from IFABP coordinates (pdb code 1icm) with residue 60 modeled as an alanine and all heteroatoms removed. The correct solution calculated using CNS (Brünger et al., 1998) revealed the molecular packing and position were nearly equivalent, but rotated 180° to that of three matching IFABP crystal lattices found previously. The initial R_{factor} was 28.9% (R_{free} 29.1%) after rigid body refinement. Furthermore, excellent electron density was observed for the N60 side chain and the entire main chain. The structure of V60N-IFABP was refined using CNS with data of 20–2.1 Å resolution accompanied by application of bulk-solvent correction and maximum likelihood weighting. The final model contains residues 1 to 131 and 73 solvent molecules. The R_{factor} is 18.9% (R_{free} 22.8%). The coordinates have been deposited in the pdb as entry 1DC9.

Computational analysis of IFABP structure

Empirical hydrogen bond (Hbond) and van der Waals (VDW) energy functions incorporated into X-PLOR 3.8 (Brünger, 1990) were used to study differences in intramolecular interactions for V60N and the other existing IFABP crystal structures. Before the estimation, coordinates for explicit hydrogen atoms were generated and energy minimized with heavy atoms fixed in place. X-PLOR uses slightly modified CHARMM parameters and topologies with increased force constants for peptide dihedrals (Brooks et al., 1983). However, since no energy minimization was carried out, the adjustments are unimportant. Normalized crystallographic B-factors and solvent-accessible surface areas were calculated for each of the IFABP crystal structures. The average B-factors for side-chain and main-chain atoms were divided by the overall average B-factor of each crystal structure to achieve normalization. This was important to correct for the dependence of B-factors on the varying quality and resolution of the x-ray diffraction data sets. Thus, the values are expressed as ratios and are unit-less. The solvent exposed surface areas were calculated using DSSP (Kabsch and Sander, 1983) and a 1.4 Å radius solvent molecule as a probe.

RESULTS

No significant differences were observed in the CD or the fluorescence spectrum of the mutant protein compared to wild-type in either the native or unfolded state (data not shown). Based on these two criteria it appeared the conformation of the V60N-IFABP had not changed significantly from the native protein. The solution results were confirmed by the crystal structure as discussed below.

The stability and reversibility of folding and unfolding of IFABP and V60N-IFABP were monitored by CD and fluorescence changes using urea as the denaturant (Fig. 2). For both proteins, the transitions were completely reversible and best fit by a simple two-state model for unfolding, indicating that no detectable population of intermediates was present at equilibrium. The transitions were not dependent on protein concentration (data not shown).

V60N-IFABP was less stable than the wild-type protein. The thermodynamic parameters for the fit to a two-state model for IFABP and V60N-IFABP are shown in Table 1. This decreased stability was surprising considering prior energy calculations consistently predicted that the protein should be somewhat more stable. The anticipated increase in stability was largely due to the apparent formation of a hydrogen bond (3.0–3.2 Å bond length) from the ND2 of the asparagine side chain to the OE1 of E51.

To determine whether the mutation also had any significant effects on the mechanism of folding, the rates of denaturation and renaturation of the mutant protein were determined by stopped-flow fluorescence. These rates are

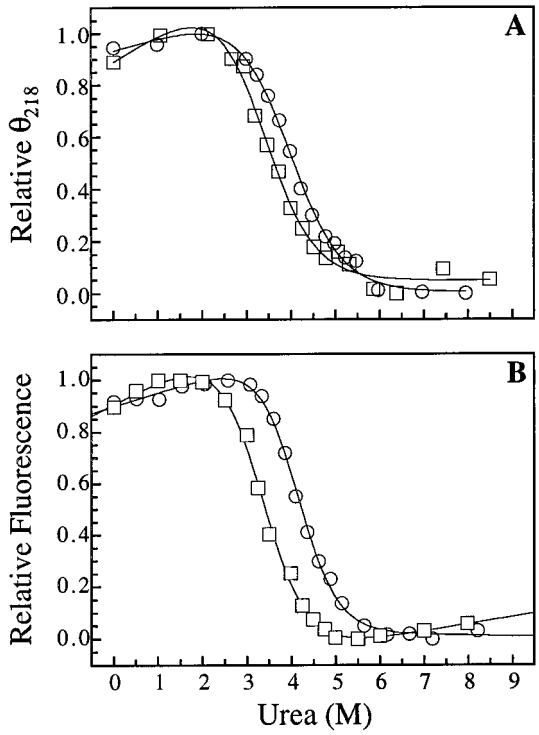

FIGURE 2 The reversible folding and unfolding of IFABP (○) and V60N-IFABP (□). (A) Circular dichroism measurements are shown as a function of urea concentration at equilibrium. The samples contained 100 μg/ml protein, 25 mM $NaPO_4$, 75 mM NaCl, and 0.1 mM EDTA at pH 7.0 with various concentrations of urea. (*B*) The intrinsic tryptophan fluorescence under the same sample conditions as (*A*) except with 11 μg/ml protein. The fluorescence data were obtained using an excitation wavelength of 290 nm and the emission was monitored at 340 nm.

shown in Fig. 3, where a comparison is made to those of wild-type IFABP. Two rates were detected during unfolding that accounted for the entire expected amplitude change (Fig. 3). Approximately 75–80% of the expected amplitude change was associated with the faster rate of unfolding. The remaining signal was associated with the slower phase. The rates and relative amplitudes were not dependent on protein concentration over a 10-fold concentration range (data not shown).

Different results were observed when the unfolding process was studied by stopped-flow CD. Only one rate was detected, which accounted for the entire expected amplitude of the transition. This rate corresponded to the faster of the two rates observed by fluorescence. The same patterns in rates and amplitudes were observed during the unfolding of wild-type IFABP with urea (lines in Fig. 4, Ropson and Dalessio, 1997; Dalessio and Ropson, 1998). Note that the rates of unfolding of the mutant protein were significantly faster than those of wild-type IFABP.

The observation of two rates by fluorescence suggested that an intermediate was present on the unfolding path:

$$\mathbf{N} \Rightarrow \mathbf{I} \Rightarrow \mathbf{U}$$

For both V60N-IFABP and IFABP, the data implied that secondary structure was lost during the unfolding of the native protein to the intermediate structure (**I**) above. No secondary structure remained to be lost as the intermediate continues to unfold.

Unlike unfolding, a significant burst phase amplitude was detected by both CD and fluorescence during refolding for both the mutant and wild-type protein (Fig. 3). This burst phase amplitude increased at lower final concentrations of denaturant. Two additional kinetic phases were observed by fluorescence during refolding. Approximately 90% of the observed amplitude change is associated with the faster rate. Only one additional phase was observed by CD during the refolding of the mutant protein (Fig. 4), although only rates between 0.1 and 10 s^{-1} can be observed by stopped-flow CD with our equipment. The rate observed by CD corresponded to the faster of the two rates observed by fluorescence. The rates and relative amplitudes were not dependent on protein concentration over a 10-fold range (data not shown).

The kinetic behavior of the mutant protein during refolding is in contrast to the wild-type protein at pH 7, for which only a single identical rate was observed by both methods. As such, the folding of V60N-IFABP appeared to be more complex than wild-type protein, perhaps including the formation of an additional molten globule-like intermediate. The spectral and kinetic properties of the intermediate observed during the folding of the mutant protein were similar to those observed for the wild-type protein at pH 10 (Dalessio and Ropson, 1998), where an intermediate with similar spectral properties was formed. Finally, the refolding of the mutant protein was faster than that of wild-type, despite being an inherently less stable protein.

The crystal structure of the mutant protein was determined to relate the significant difference in the stability between V60N-IFABP and wild-type to specific structure changes and to confirm that the mutant protein maintained the native fold. A summary of the crystallographic statistics is given in Table 2. It is a well-determined crystal structure by all criteria. The conformation of V60N-IFABP is shown in Fig. 1, where the secondary structure is labeled in a manner similar to other family members. As expected, the overall conformation of the mutant is essentially that of existent IFABP structures.

The atomic coordinates of V60N-IFABP were superimposed with all published IFABP crystal structures after minimization by the method of least squares to optimize the coordinate overlap of the C_α atoms. There were six structures found in five pdb entries: 1ICM (IFABP complex with myristate), 1ICN (R106Q mutant), 1IFC models A and B (two alternate conformations of apo-IFABP), 1IFB (apo-IFABP), and 2IFB (IFABP-palmitate complex). The resolution of the x-ray data for each structural determination was 1.5, 1.7, 1.2, 2.0, and 2.0 Å, respectively, compared to the 2.1 Å of this study. Following in the same order, the

TABLE 1 Thermodynamic parameters calculated for the urea-induced unfolding of IFABP and V60N-IFABP

Protein	ΔG_{H_2O} (kcal/mol^{-1})	$\Delta\Delta G_{H_2O}$ (kcal/mol^{-1})	m_G (kcal/mol^{-1}/M^{-1})	Midpoint (M)
IFABP				
Urea (θ_{218})	4.28 + 0.27		−1.04 + 0.06	4.10 + 0.04
Urea (F_{340})	4.79 + 0.22		−1.13 + 0.07	4.24 + 0.03
V60N-IFABP				
Urea (θ_{218})	3.39 + 0.25	0.75	−1.01 + 0.06	3.36 + 0.06
Urea (F_{340})	4.17 + 0.31	1.67	−1.24 + 0.09	3.36 + 0.04

mean rms difference for the 131 C_α atoms were 0.3, 0.4, 0.5, 0.6, 0.7, and 0.6 Å. The cross-validated coordinate error estimated for the V60N structure is 0.3 Å (Kleywegt et al., 1994). It is important to note that the same analysis between any of the IFABP structures, excluding the V60N, results in comparable or even greater rms coordinate differences. The unit cell parameters and crystal packing of the two structures with the largest differences, 1IFB and 2IFB, differ from those of the V60N mutant and the other crystal structures.

For a more localized comparison, the rms distance is plotted by residue for all atoms (*top bars*) and main-chain atoms (*bottom bars*) in Fig. 5 for each paired structure. Only the CB atom of the N60 side chain in V60N was included in the all-atom calculation. Similarly, only equivalent atoms were used at position 106 in the trial with 1ICN, a R106Q mutant structure of IFABP. The two uppermost histograms depict the local differences between V60N and the 1IFB and 2IFB structures. The region around residues 24–26 of the second helix contained relatively large conformational differences in both cases. These residues are involved in crystal packing interactions not present in the remaining structures and the differences complicate any analysis.

The bottommost four histograms should not reflect packing considerations. Regarding two molecules of apo-IFABP (1IFC A and B in Fig. 5), the conformation appeared to be significantly different for a few residues around D74 and E85. The most significant variation was around D74 in the turn connecting strands βE and βF, 14 amino acids from the mutation site. These larger differences between main-chain positions were mainly traceable to changes in the backbone torsional angles ϕ and ψ. The conformational difference of the C-terminal residue 131 of both apo-structures were likely in error due to bad contacts with symmetry-related molecules (residue 24) within the crystal. Finally, no substantial local differences were found between the V60N and IFABP with myristate or the R106Q mutant structures. Most importantly, no significant differences were detected between these structures at or near residue 60, the mutation site.

The conformation of V60N-IFABP around N60 is shown in Fig. 6. For comparative purposes, the structure of IFABP (1ICM) at that location is included and colored green. IFABP (1ICM) represents the crystal coordinates most similar to the V60N-IFABP structure. The position and orientation of the asparagine side chain atoms were nearly identical to those predicted from modeling. The designed

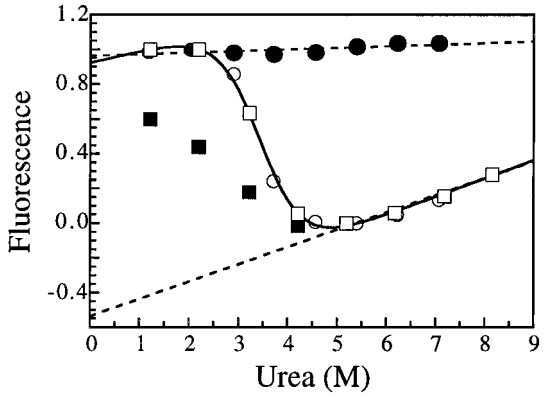

FIGURE 3 Initial and final intensities from stopped-flow fluorescence studies of the folding and unfolding of V60N-IFABP. The equilibrium endpoints obtained from unfolding (○) and refolding (□) stopped-flow experiments. The line through the data is the fit to a two-state model for equilibrium folding and unfolding. Closed symbols represent the initial fluorescence intensity at the start of the kinetic transition for unfolding (●) and refolding (■). Dashed lines indicate the expected initial fluorescence intensity based on the extrapolated native and unfolded baselines in this instrument.

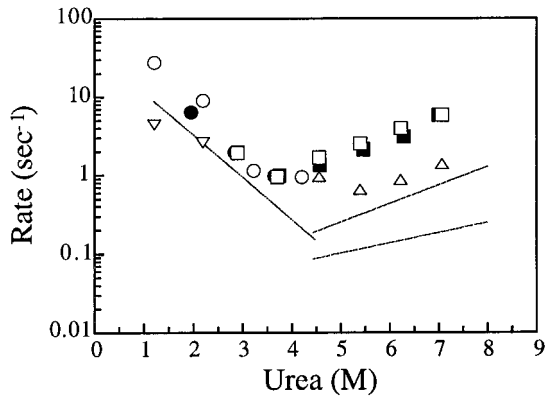

FIGURE 4 The folding and unfolding rates of V60N-IFABP. Two rates of unfolding were observed by stopped-flow integrated fluorescence (□, △) and one by CD (■). The single refolding rate observed by CD (●), and the faster and slower rates of refolding observed by fluorescence (○, ▽). The final protein concentration was 0.26 mg/ml. The lines show the comparable folding and unfolding rates for IFABP at pH 7.

TABLE 2 X-ray data and refinement statistics

Data collection	
Space group	$P2_1$
Unit cell	a = 36.64, b = 52.37, c = 31.59 Å, β = 90.92
Resolution limit (Å)	20 –2.09
Observations	19,796 (779)
Unique reflections	6400 (447)
Redundancy	3.1 (1.7)
Ave I/σ_1	23.9 (1.4)
Completeness (%)	91 (38.2)
R_{merge} (°)	4.7 (15.1)
Refinement	
Resolution range (Å)	20–2.1
R_{factor} (%)	18.9
R_{free} (%)	22.8
R.m.s. bond lengths (Å)	0.007
R.m.s. bond angles (°)	1.3
R.m.s. dihedrals (°)	26.0

The values found in parentheses are those for the highest resolution bin of x-ray data.

hydrogen bond between the side chains N60 and E51 appeared to be present, although the distance between participating atoms was 3.4 Å and the angles involved were not optimal. The accommodation of asparagine rather than the native valine in packing with neighboring residues from the preceding β-strand, especially V49, may in part account for small differences in the main-chain torsional angles for residue 59. However, there were no major conformational changes in the V60N structure that were obviously coupled to the mutation of valine to asparagine. Furthermore, no significant changes were observed in the bound water structure within 4 Å of the mutation site (not shown for clarity).

Because of the similarity in conformation, Hbond and VDW energy terms were calculated between atomic coordinates (see Methods) in a further attempt to find a basis for the destabilization of the mutant protein. The results are reported in Fig. 7, *A* and *B*. Although the units are given in kcal/mol, they are essentially arbitrary. The average differences for these enthalpic, noncovalent interactions are shown in stacked histograms on a residue-by-residue basis for main chain (*solid bars*) and side chain (*open bars*). The rows directed above zero indicate that lower and more stabilizing energies were found in the V60N structure. All red bars indicate that the mean difference was more than three times greater than the standard deviation, a level judged significant.

Note that few significant differences occurred between the mutant and other IFABPs, as shown in Fig. 7, *B* and *C*. All of the major differences in hydrogen bond energies involved side-chain atoms (*open red bars*) at the molecular surface of the protein, including E19, R28, H33, N35, E43 and E107. As the analysis only considers intramolecular interactions, no account was made of (de)solvation changes unique to V60N′s surface. The hydrogen bond between the side chains of N60 and E51 was very weak. The calculated energy was −0.6 kcal/mol for this bond, compared to −2.1 and −3.0 kcal/mol for the two hydrogen bonds involving the main chain of position 60. In the estimation of VDW interactions, the side chains of D59 and T81 appeared to have a significant destabilizing influence in the crystal structure of V60N-IFABP. D59 presses against K50, another residue with poorer packing in the mutant. Residue T81 was partly uncovered by a small shift in β-turn conformation centered at G65. However, the VDW energies for the mutant asparagine were surprisingly low and indicated more optimized packing than for the wild-type valine. In fact, the atomic packing in V60N as a whole appeared energetically lower than that of the other IFABPs.

A summation of the total energies for each structure is found in Table 3. The energies from packing interactions between molecules related by the crystal lattice are not reported in Fig. 7, although they are included under the heading "XTAL VDW" in Table 3. These packing contributions appeared to be ~6–15% of the total "conformational energy." However, some of these values were highly suspect due to interaction energies higher than the norm because of several unresolved atomic contacts in pdb entries 1ICM, 1IFC, and to a lesser extent, 1IFB. The inclusion of hydrogen atoms that were not considered in the original structural refinement only affected this result in the case of 1IFB. The total energies differed by ~29%. However, the energy total for V60N is more negative, suggesting greater stabilization than that of any of the other structures. These calculations on the crystal structure agreed with the original modeling of this mutation. However, the solution studies described above clearly indicated that the V60N-IFABP was less stable than the wild-type protein.

Two explanations for the discrepancy were immediately apparent. The error can be attributed to inaccuracies in the coordinates and in the methods used to estimate the coordinate conformational energy. Alternatively, the calculations omitted additional substantial energies. To assess potential entropic factors, normalized crystallographic B-factors and solvent-accessible surface areas were calculated (see Methods) for each of the six structures. For both, the average difference between the wild-types versus the mutant is shown in the bottommost two panels of Fig. 7.

Small regions of lower values (*upward bars*) in the calculations of normalized B-factor differences are found in the V60N structure for residues comprising helix α2 and the C-termini (Fig. 7 *C*). The mutation site was more disordered than in the native protein, as shown by negative bars. Nearly all V60N′s amino acids between D34 and roughly A124, however, have higher B-factors when normalized by the overall average for each structure. In the latter case, all differences more than three standard deviations in value were colored red. One observation is that in V60N the van der Waals packing interactions for the same region are

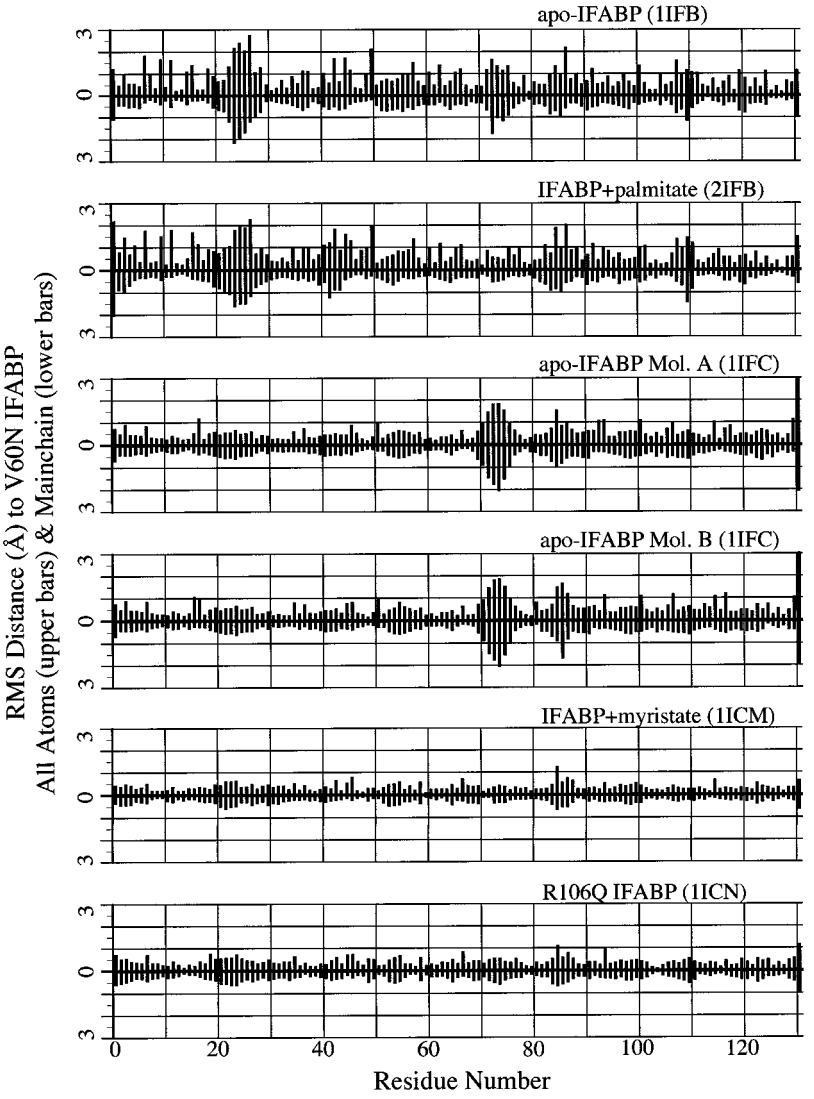

FIGURE 5 Coordinate RMS distance comparison of V60N-IFABP to wild-type IFABP structures. The histograms show the mean distance difference for all atoms (*top bars*) and main-chain atoms (*bottom bars*) by residue. To facilitate plotting, distance differences between main-chain atoms are given a negative value. The comparisons were made between V60N and six IFABP crystal structures as described in the Methods section. The wave-like or nodal appearance of the differences is due to increasing variance on the ends of the connecting anti-parallel β-strands, all of roughly the same length.

optimal. The greatest differences seem to be centered on residues L72–L78, indicating entropic destabilization of the β-turn formation connecting the E and F β-strands.

A considerable degree of the V60N structure's surface area was more solvent-exposed than that found in the other IFABP studies; this is shown by the amplitude and number

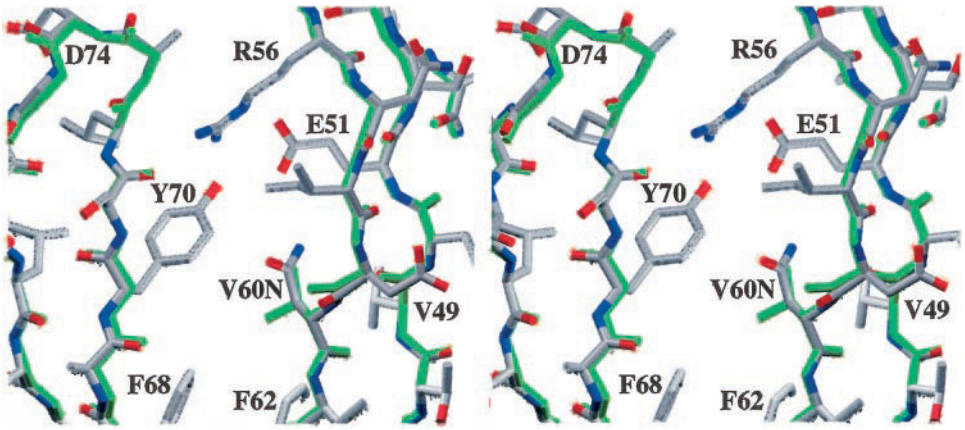

FIGURE 6 Local conformation about the site of the V60N mutation. The stereo drawing contains a stick model representation of an overlay of the crystal structure of V60N and one of the wild-type crystal structures. The latter is colored green; atoms in V60N-IFABP are color-coded with C atoms in gray, N atoms in blue, and O positions in red. A few key residues are numbered according to the amino acid sequence.

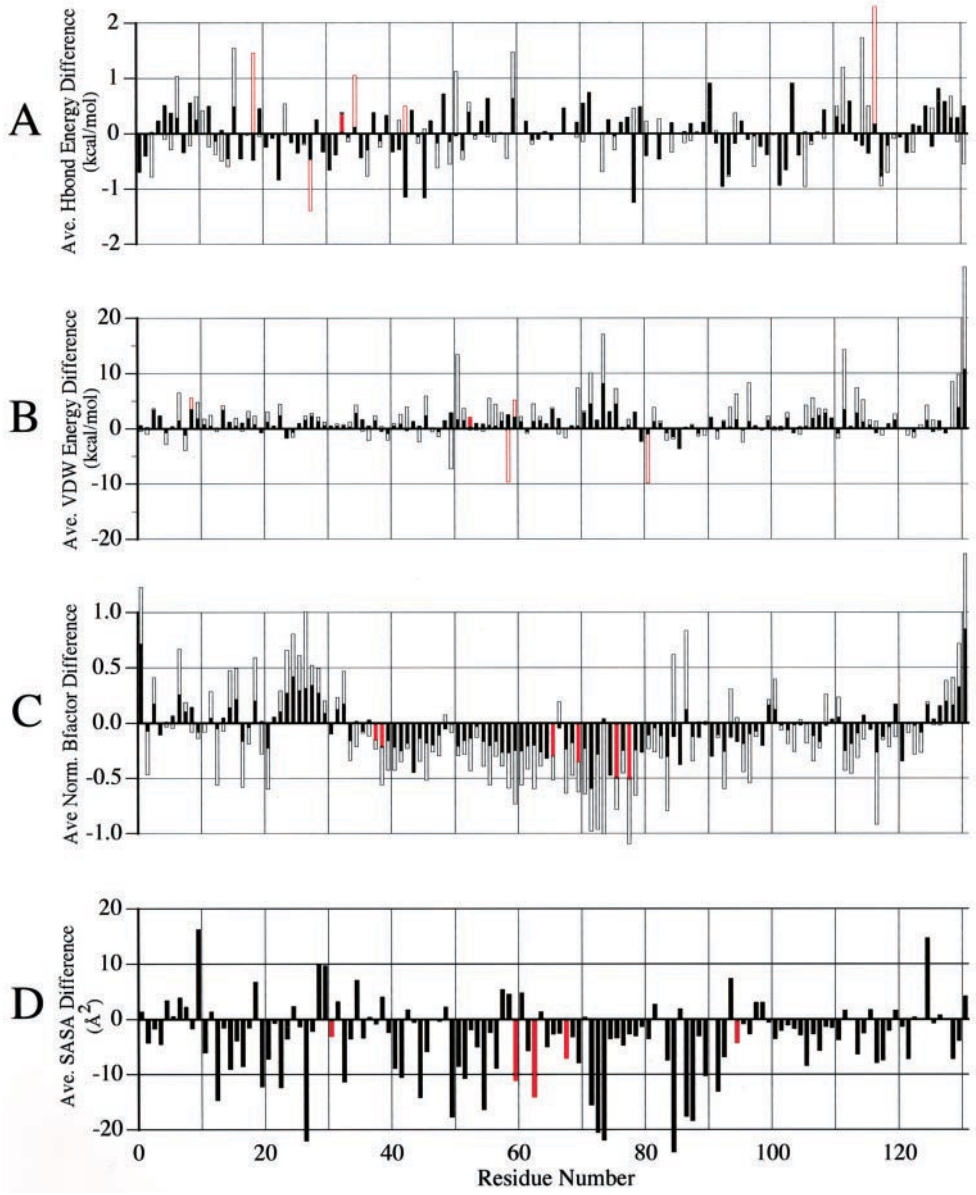

FIGURE 7 Average differences in conformational energy factors between V60N and other IFABP structures. The results of average differences in hydrogen bond (Hbond) and van der Waals (VDW) energy terms are shown on a residue-by-residue basis for main chain (*solid bars*) and side chain (*open bars*) in (*A*) and (*B*) (see Methods). The energy units are kcal/mol, but the scale is arbitrary. The negative bars indicate lower and more stabilizing energies were found for the V60N structure on average over six comparisons. The red bars indicate that the mean difference was more than three times greater than the standard deviation. The average differences for normalized crystallographic B-factors and solvent-accessible surface areas (SASA) are displayed in a similar manor in (*C*) and (*D*), although the SASA differences are only shown for the entire residue. Negative values indicate locations for which the V60N structure was either more disordered (*C*) or the solvent surface more solvent-exposed (*D*).

of negative bars in Fig. 7 *D*. In particular, N60 itself was more exposed than the conformation of V60 found in the wild-type structures. The neighboring residues A73 and L78 were also more exposed by a significant amount (more than three standard deviations above the mean). Although not deemed significant compared to V60N, residues in β-turns around D74 and E85 also varied greatly in solvent-exposed surface area between IFABP structures.

DISCUSSION

The V60N mutation of IFABP was originally made to determine the contribution of this cavity surface site to ligand binding specificity (D. Cistola, personal communication). Energy minimization and molecular dynamics simulations consistently predicted that V60N-IFABP would be as much as 10–25% more stable than wild-type, depending on the force field used. The predicted increase in stability

TABLE 3 Estimation of energies in IFABP crystal structures and V60N-IFABP

IFABP Structure	Conformational Energy–Relative Scale (kcal/mol)					
	HBONDS	VDW	XTAL	VDW	TOTAL	
V60N	1DC9	−239 (24%)	−692 (69%)	−71	(7%)	−1002
Apo	1IFC B	−243 (25%)	−602 (61%)	8019	[−139 (14%)]*	−984*
Apo	1IFC A	−242 (25%)	−618 (63%)	5545	[−118 (12%)]*	−978*
Myristate	1ICM	−249 (28%)	−588 (66%)	2103	[−54 (6%)]*	−891*
R106Q	1ICN	−251 (30%)	−510 (61%)	−81	(10%)	−842
Palmitate	2IFB	−241 (29%)	−540 (65%)	−53	(6%)	−834
Apo	1IFB	−196 (28%)	−409 (58%)	64	[−105 (15%)]*	−710*

Energy estimates for V60N-IFABP and six crystal structures of IFABP were calculated as described in Methods. "XTAL VDW" refers to van der Waals interactions between equivalent molecules related by crystal lattice symmetries. The values in parentheses are percentages of the total energy.
*Coordinates containing atomic contacts due to crystal symmetry. The energies within the brackets are determined by ignoring all residue interactions over 5 kcal/mol in a second summation. The corrected energies were used in calculations of total energies. The residues removed from consideration in 1IFCA and B are 24, 25, 131; in 1ICM they are 19, 24, 25, 29, 30, 42, 44, 46, 88, 97, 98, 101, 109, 121, 130, 131; in 1IFB they are 7, 10, 12, 29, 63, 77, 81, 83.

was associated with an additional hydrogen bond formed between N60 and E51. Experimental results showed that the thermodynamic stability of the V60N mutation was less than that of the wild-type protein. The crystal structure of the V60N-IFABP was determined to attempt a correlation of stability with conformation and to confirm that the mutant protein had assumed the same structure as the wild-type protein. Because the V60N mutation only involved a two-atom change, our expectation was that any differences would be due to the shift in polarity and/or the location of the mutation.

Because the wild-type and V60N proteins have nearly identical spectroscopic properties, it was not surprising that the V60N structure was basically the same as the wild-type protein. In fact, when the V60N crystal structure was extensively compared with six crystallographic IFABP sets of coordinates in five pdb entries, the distance between equivalent atomic coordinates after their superposition was only slightly above that of their estimated experimental error. However, using this ensemble of conformational data provided a mechanism for evaluating the significance of the calculation, and partially accounted for the small errors found in all coordinate sets. Local regions of conformational difference were found by this comparison in the polypeptide forming two β-turns connecting the β-strands E and F, and F and G, that were not due to crystal packing. Neither site was obviously associated with the mutation site at position 60 in the crystal structure.

To evaluate the stabilization due to protein interactions, CHARMM energy functions as implemented by XPLOR were used directly with the x-ray coordinates. Comparisons of the energy terms resulting from non-covalent interactions, as shown in Fig. 7, *A* and *B*, provided little clue as to where to attribute the mutant's decrease in stability. The hydrogen bond that was initially predicted from modeling was present, but the length and the geometry of the interaction were poorer than those of the model protein; thus the hydrogen bond was energetically weak. The simulations were based on the 1IFC structure, which has a different rotamer conformation for the side chain of E51 than that found in the mutant structure. This conformation in the mutant protein moves the terminal carbonyl of the E51 side chain further from the amide group of N60 than that in the modeled structure. The alternative rotamer conformation was not sampled in either of the short molecular dynamics trajectories that were run. However, even with this poor bond geometry, the calculated non-covalent interactions of the crystal structure predicted that the mutant should be more stable by 2–29%, depending upon which IFABP structure the comparison was made to. One possibility is the destabilization was largely entropic in nature.

This hypothesis was supported by structural differences found by calculation of normalized B-factors and solvent-exposed surface areas, both entropic related quantities. The relationship of protein stability to the atomic solvation parameters and accessible surface area has been noted for some time (Eisenberg et al., 1989). The results, shown in Fig. 7, *C* and *D*, revealed a notable bias with V60N-IFABP having increased atomic B-factors after normalization and increased accessible surface area compared to the other six IFABP structures. The major contribution to this change appears in the region bounded by roughly V49 and F93, particularly the βF-βG and βG-βH turns. This region of IFABP includes many of the hydrophobic residues of the protein. Such differences were not readily apparent when the stick models of the overlaid proteins were examined.

Therefore, one explanation for the destabilization found in the mutant form may be related to a finding of greater positional disorder despite more efficient atomic packing. Another contributing factor to the decreased stability in the mutant may be the loss of local steric constraints imposed on the backbone configuration by the C_β-branched side chain of valine. Valine produces the largest decrease in the configurational entropy of the backbone, ~4.4 cal/K · mol. This value is ~1.1 cal/K · mol more than that of asparagine. These values were determined in a mutant study where differences in peptide stability could be attributed solely to configurational entropy (D'Aquino et al., 1996).

The mutation also had significant effects on the rate of folding and unfolding. Unfolding was accelerated by a factor of 10, whereas the rate of refolding for the major observed phase was accelerated by a factor of 5. The simplest explanation for these results is that the mutation lowers the activation energy barriers for transitions between the native and intermediate and intermediate and unfolded states, allowing both the folding and unfolding processes to proceed faster. This residue position is adjacent to an apparent folding initiation site (Ropson and Frieden, 1992; Ropson and Dalessio, 1997), which is thought to include F62.

One purely speculative hypothesis on the cause of the more rapid folding again involves the β-branched nature of valine. Folding may be related to the process of seeking the optimal collection of ϕ and ψ angles. Due to the β-branched nature of the valine side chain, the rotation about these angles for residues near the valine 60 location may be more difficult. The replacement of the valine with the C_δ-branched asparagine might alleviate this effect, lowering the transition state barriers into and out of the intermediate state, making the folding and unfolding reactions proceed faster.

The authors acknowledge grants for computational studies from the Minnesota Supercomputer Institute. L.J.B. and J.T. thank Judy Bratt for the preparation of suitable crystals. The University of Minnesota part of the study was supported by National Institutes of Health Grant GM13925. The Penn State University portion of the study was supported by National Science Foundation Grant MCB-9405282.

REFERENCES

Banaszak, L., N. Winter, Z. Xu, D. A. Bernlohr, S. Cowan, and T. A. Jones. 1994. Lipid-binding proteins: a family of fatty acid and retinoid transport proteins. *Adv. Protein Chem.* 45:89–151.

Bass, N. M. 1993. Cellular binding proteins for fatty acids and retinoids: similar or specialized functions. *Mol. Cell. Biochem.* 123:191–202.

Bernlohr, D. A., M. A. Simpson, A. Vogel-Hertzel, and L. J. Banaszak. 1997. Intracellular lipid-binding proteins and their genes. *Annu. Rev. Nutrition.* 17:277–303.

Brooks, C. L. III, M. Karplus, and B. M. Pettitt. 1983. CHARMM: a program for macromolecular energy minimization and dynamics calculations. *J. Comput. Chem.* 4:187–217.

Brünger, A. T. 1990. XPLOR Version 3.1: A System for Crystallography and NMR. Yale University Press, New Haven, CT.

Brünger, A. T., P. D. Admas, G. M. Clore, W. L. Delano, P. Gros, R. W. Grossekunstleve, J. S. Jaing, J. Kuszewski, M. Nilges, N. S. Pannu, R. J. Read, L. M. Rice, J. Simonson, and G. L. Warren. 1998. Crystallography and NMR system—a new software suite for macromolecular structure determination. *Acta Crystallogr. D.* 54:905–921.

Burns, L. L., P. M. Dalessio, and I. J. Ropson. 1998. The folding mechanism of three structurally similar β-sheet proteins. *Proteins.* 33: 107–118.

Dalessio, P. M., and I. J. Ropson. 1998. pH dependence of the folding of intestinal fatty acid binding protein. *Arch. Biochem. Biophys.* 359: 199–208.

Dalessio, P. M., and I. J. Ropson. 2000. β-Sheet proteins with nearly identical structures have different folding intermediates. *Biochemistry*. In press.

D'Aquino, J. A., J. Gómez, V. J. Hilser, K. H. Lee, L. M. Amzel, and E. Freire. 1996. The magnitude of the backbone conformational entropy change in protein folding. *Proteins.* 25:143–156.

Eisenberg, D., M. Wesson, and M. Yamashita. 1989. Interpretation of protein folding and binding with atomic solvation parameters. *Chemica Scripta.* 29A:217–221.

Gantz, I., S. F. Nothwehr, M. Lucey, J. C. Sacchettini, J. DelValle, L. J. Banaszak, M. Naud, J. I. Gordon, and T. Yamada. 1989. Gastrotropin: not an enterooxyntin but a member of a family of cytoplasmic hydrophobic ligand binding proteins. *J. Biol. Chem*. 264:20248–20254.

Gordon, J. I., D. H. Alpers, R. K. Ockner, and A. W. Strauss. 1983. The nucleotide sequence of rat liver fatty acid binding protein mRNA. *J. Biol. Chem.* 258:3356–3363.

Howard, A. J., G. L. Gilliland, B. C. Finzel, T. L. Poulos D. H. Ohlendorf, and F. R. Salemme. 1987. The use of an imaging proportional counter in macromolecular crystallography. *J. Appl. Crystallogr.* 20:383–387.

Kabsch, W., and C. Sander. 1983. Dictionary of protein secondary structure: pattern recognition of hydrogen-bonded and geometrical features. *Biopolymers.* 22:2577–2637.

Kleywegt, G. J., T. Bergfors, H. Senn, P. LeMotte, B. Gsell, K. Shudo, and T. A. Jones. 1994. Crystal structures of cellular retinoic acid binding proteins I and II in complex with all-trans-retinoic acid and a synthetic retinoid. *Structure.* 2:1241–1258.

Lowe, J. B., J. C. Sacchettini, M. Laposata, J. J. McQuillan, and J. I. Gordon. 1987. Expression of rat intestinal fatty acid binding protein in *Escherichia coli. J. Biol. Chem.* 262:5931–5937.

Mannervik, B. 1982. Regression analysis, experimental error, and statistical criteria in the design and analysis of experiments for discrimination between rival kinetic models. *Methods Enzymol.* 87:370–389.

Motulsky, H. J., and L. A. Ransnas. 1987. Fitting curves to data using nonlinear regression: a practical and nonmathematical review. *FASEB J.* 1:365–374.

Pace, C. N. 1986. Determination and analysis of urea and guanidine hydrochloride denaturation curves. *Methods Enzymol.* 131:266–280.

Ropson, I. J., and P. M. Dalessio. 1997. Fluorescence spectral changes during the folding of intestinal fatty-acid binding protein. *Biochemistry.* 36:8594–8601.

Ropson, I. J., and C. Frieden. 1992. Dynamic NMR spectral analysis and protein folding: identification of a highly populated folding intermediate of rat intestinal fatty acid-binding protein by ^{19}F NMR. *Proc. Natl. Acad. Sci. USA.* 89:7222–7226.

Ropson, I. J., J. Gordon, and C. Frieden. 1990. Folding of a predominantly β-structure protein: rat intestinal fatty acid binding protein. *Biochemistry.* 29: 9591–9599.

Sacchettini, J. C., L. J. Banaszak, and J. I. Gordon. 1990. Expression of rat intestinal fatty acid binding protein in *E. coli* and its subsequent structural analysis: a model for studying the molecular details of fatty acid-protein interaction. *Mol. Cell. Biochem.* 98:81–93.

Sacchettini, J. C., J. I. Gordon, and L. J. Banaszak. 1989. Crystal structure of rat intestinal fatty-acid binding protein: refinement and analysis of the *Escherichia coli* derived protein with bound palmitate. *J. Mol. Biol*. 208:327–339.

Santoro, M. M., and D. W. Bolen. 1988. Unfolding free energy changes determined by the linear extrapolation method: unfolding of phenylmethanesulfonyl α-chymotrypsin using different denaturants. *Biochemistry.* 27:8063–8068.